IEEE Photonics Journal
An IEEE Photonics Society Publication

Coupling-Strength-Independent Long-Period Grating Designs for THz-Bandwidth Optical Differentiators

Volume 5, Number 2, April 2013

Reza Ashrafi, Student Member, IEEE
Ming Li, Member, IEEE
José Azaña, Member, IEEE

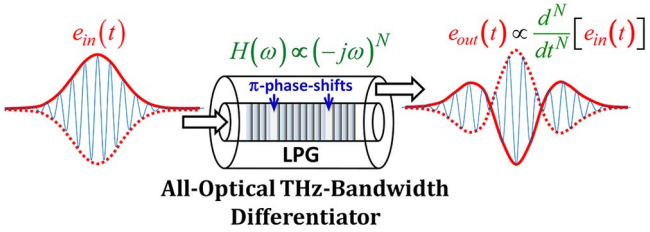

DOI: 10.1109/JPHOT.2013.2256117
1943-0655/$31.00 ©2013 IEEE

IEEE photonics SOCIETY

IEEE

Coupling-Strength-Independent Long-Period Grating Designs for THz-Bandwidth Optical Differentiators

Reza Ashrafi, *Student Member, IEEE*, Ming Li, *Member, IEEE*, and José Azaña, *Member, IEEE*

Institut National de la Recherche Scientifique—Energie, Matériaux et Télécommunications (INRS-EMT), Montréal, QC H5A 1K6, Canada

DOI: 10.1109/JPHOT.2013.2256117
1943-0655/$31.00 ©2013 IEEE

Manuscript received March 19, 2013; accepted March 26, 2013. Date of publication April 3, 2013; date of current version April 10, 2013. Corresponding author: R. Ashrafi (e-mail: ashrafi@emt.inrs.ca).

Abstract: A novel design of THz-bandwidth all-optical arbitrary-order temporal differentiators using long period fiber/waveguide gratings (LPGs) is proposed and numerically demonstrated. The proposed technique is based on the first-order Born approximation approach in LPGs. We show that an *N*th-order optical differentiator can be implemented based on an LPG incorporating N π-phase shifts along its length and operating in the cross-coupling mode. The proposed design has a strong tolerance against practical fluctuations in the grating parameters, e.g., as induced during the fabrication process or by environmental fluctuations. In particular, this LPG design solution is essentially insensitive to variations in the grating coupling strength.

Index Terms: All-optical devices, fiber optics components, ultrafast processing, optical differentiation.

1. Introduction

All-optical devices and circuits for computing, networking, and data processing are being practically developed to surpass the electronics speed [1]. Optical differentiators are of fundamental interest as basic building blocks in ultrahigh-speed all-optical analog/digital signal processing and computing circuits [1], [2]. An *N*th-order optical differentiator (NOOD) is a device that calculates the *N*th-time (i.e., $N = 1, 2, 3, \ldots$) derivative of an arbitrary input optical signal (i.e., temporal complex envelope). NOODs have been already employed for a wide range of applications, including generation and processing of ultrahigh bit-rate ($\sim$Tbit/s) optical communication signals [3], ultrashort optical pulse shaping [2], and methods for the characterization and measurement of optical devices and signals [4], [5].

NOODs have been implemented using microring resonators [6], and fiber/integrated-waveguide Bragg gratings [7]–[10]. However, the frequency-bandwidth (speed) of operation for these cases is typically limited to a few hundreds of gigahertz. Faster speeds, i.e., processing bandwidths of a few THz, have been achieved using uniform long period fiber gratings (LPGs) for implementation of 1st-order optical differentiators (i.e., NOODs, $N = 1$) [11]. For this purpose, the LPG should operate in *full-coupling condition* [11]. NOODs $(N = 1)$ with larger operation bandwidths, i.e., a few tens of THz, have also been recently demonstrated based on an all-fiber wavelength-selective directional coupler [12]. The more general case of higher-order (i.e., $N > 1$) THz-bandwidth NOODs has been proposed and demonstrated using an LPG incorporating $N - 1$ π-phase shifts, working in the core-to-core operation mode [13]. A critical drawback of these previous approaches [11]–[13] is that they

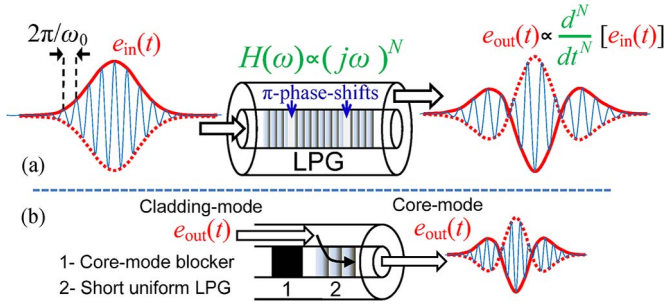

Fig. 1. (a) LPG configuration for the proposed ultrafast NOODs (the case of $N = 2$ is illustrated here). (b) A fiber-optic approach previously demonstrated [18], for efficiently capturing the cladding-mode signal by using (1) a core-mode blocker, cascaded with (2) a short and broadband uniform LPG with a strong coupling strength.

are extremely sensitive to small variations in the grating parameters, particularly variations in the coupling strength, which must be fixed to satisfy very specific conditions. To give an example, the aforementioned *full-coupling condition* for an LPG-based NOOD, $N = 1$, requires that the coupling-length product in the grating must be fixed to exactly satisfy the equation $k \cdot L = \pi/2$, where k is the grating coupling coefficient and L is the total grating length. In general, it is challenging to fabricate a grating with a coupling strength strictly satisfying this condition; additionally, the differentiator performance will be greatly affected by any variation in the coupling characteristics, e.g., easily induced by environmental fluctuations. To overcome this problem, a single phase-shifted LPG working in the cross-coupling (e.g., fiber core-to-cladding) operation mode for implementation of 1st-order differentiator has been proposed [14].

In this paper, we introduce a novel realization of THz-bandwidth NOODs, $N = 1, 2, 3, 4, \ldots$, based on LPGs, generalizing the previous approach [14]. Our generalized technique is based on a recently introduced linear-filter synthesis approach in LPGs, the so-called superluminal space-to-time mapping [15], [16]. We show that, in general, a NOOD, $N = 1, 2, 3, 4, \ldots$, can be implemented by suitably locating N π-phase shifts in a uniform-period LPG working in the cross-coupling operation mode. Moreover, we carry out a comprehensive numerical analysis of the designed devices, proving that this LPG design solution is nearly insensitive to variations in the grating coupling strength over extremely large coupling ranges, thus dramatically relaxing the needed specifications for practical realization of these devices.

2. Operation Principle

For implementation of a NOOD, one can use a linear optical filter with a frequency response of $H(\omega) \propto (-j\omega)^N$, with $\omega = \omega_{opt} - \omega_0$. ω_0 is the carrier angular frequency of the input temporal complex envelope, i.e., $e_{in}(t)$ in Fig. 1(a), to be processed. ω and ω_{opt} are the baseband and optical angular frequency variables, respectively. We also define *Frequency* $= \omega/2\pi$ as the baseband frequency variable.

A general architecture of the proposed LPG-based NOOD is illustrated in Fig. 1(a). To implement a NOOD, N suitably located π-phase shifts are required along the LPG length. An important practical consideration concerns the fact that the input and output signals must be carried by two different waveguide modes. In an integrated-waveguide approach [17], the device could be practically implemented by using two physically separated single-mode optical waveguides. All-fiber LPGs are typically based on coupling between the core mode and a cladding mode. The signal in the cladding mode can be efficiently extracted using several different techniques, e.g., a core-mode blocker combined with a short strong uniform LPG inducing undistorted cladding-to-core coupling over the entire spectral bandwidth of interest [18], or by splicing a suitably misaligned fiber [19]. In this paper, without loss of generality, we consider the case of a fiber LPG implementation [18], [19].

3. Theoretical Principles of the Proposed Phase-Shifted LPG Designs

Our technique for realization of the target device spectral response, i.e., $H(\omega)$, is based on syn, thesizing the corresponding time-domain impulse response of the NOODs (i.e., $N = 1, 2, 3, 4, \ldots$). The grating profile that is needed to achieve the target time-domain impulse response is obtained through a fairly straightforward design approach based on the first-order Born approximation in LPGs [15], [16], referred to as superluminal space-to-time mapping, where the space-domain complex grating apodization profile is a mapped version of the desired LPG time-domain impulse response.

3.1. NOOD Temporal Impulse Response

First- and higher-order time derivative of an arbitrary input signal $a(t)$ (temporal complex envelope) can be expressed using the following central-division difference equations [20]:

$$\frac{\partial a(t)}{\partial t} \propto a(t-\tau) - a(t+\tau) \tag{1a}$$

$$\frac{\partial^2 a(t)}{\partial t^2} \propto a(t-2\tau) - 2a(t) + a(t+2\tau) \tag{1b}$$

$$\frac{\partial^3 a(t)}{\partial t^3} \propto a(t-3\tau) - 3a(t-\tau) + 3a(t+\tau) - a(t+3\tau) \tag{1c}$$

$$\frac{\partial^4 a(t)}{\partial t^4} \propto a(t-4\tau) - 4a(t-2\tau) + 6a(t) - 4a(t+2\tau) + a(t+4\tau). \tag{1d}$$

In these formulations, referred to as Euler's approximations, the time step τ defines the differentiation operation bandwidth $(\propto 1/\tau)$. To achieve a larger operation bandwidth, a shorter (faster) time step τ is required. We rewrite these Euler's formulations (1a)–(1d) as a discrete-time finite-impulse-response (FIR) filter $h(t)$ convolved with the input signal $a(t)$, as follows:

$$\frac{\partial^N a(t)}{\partial t^N} \propto a(t) \otimes h(t) \tag{2}$$

$$h(t) = \sum_i p_i \delta(t + \tau i) \tag{3}$$

where $\delta(t)$ is the Kronecker delta, i is an integer number, and $\otimes$ denotes convolution. The (positive or negative) coefficients p_i are the weights of the successive impulse-response terms. These coefficients p_i are those factors defined in (1) for each target Nth-order $(N = 1, 2, 3, 4)$ time derivation. Fig. 2(a) presents the ideal $h(t)$ (i.e., complex envelope of the temporal impulse response) of a NOOD (i.e., $N = 1, 2, 3, 4$), as expressed in (3). Fig. 2(b) and (c) respectively show two groups of practically realizable "$h(t)$" based on different but equivalent designs of impulse responses for implementation of the Nth-order differentiation.

The *areas* of the positive and negative parts of the $h(t)$ profiles (i.e., value of the cumulative integral of the impulse-response over the corresponding period) are proportional to the corresponding p_i factors [see illustrations in Fig. 2(b) and(c)]. The impulse responses in Fig. 2(b) are designed assuming a uniform sampling period, which translates into the need for different impulse-response amplitudes. In contrast, the impulse responses in Fig. 2(c) emulate the same p_i factors (i.e., same areas) but assuming a uniform impulse-response amplitude, thus requiring nonuniform sampling periods. Notice also that the processing bandwidth in the proposed designs is essentially determined by the inverse of the longest sampling period along the impulse response. In other words, to implement the target differentiation operation with a sufficiently high precision, the longest sampling period in $h(t)$ should be much shorter than the fastest temporal variation of the input signal $a(t)$ to be processed.

The designed practically realizable impulse responses shown in Fig. 2(c) are used in this paper to implement all-optical Nth-order differentiators based on phase-shifted LPGs. The impulse response designs in Fig. 2(b) for implementation using LPGs would require a precise relative variation of the grating coupling strength along the device length. In contrast, the impulse response designs in

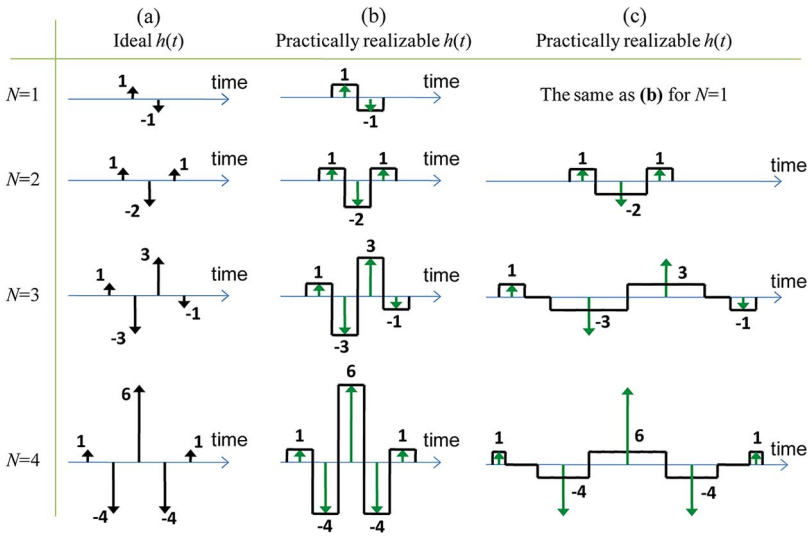

Fig. 2. Ideal (a) and practically realizable (b), (c) impulse responses (temporal complex envelope) of an Nth-order (i.e., $N = 1, 2, 3, 4$) optical differentiator. The designed impulse responses in (c) are implemented in this work based on the proposed phase-shifted LPGs. The impulse response designs in (b) for implementation using LPGs would require a precise relative variation of the grating coupling strength along the device length. In contrast, the impulse response designs in (c) can be implemented based on LPGs with constant coupling coefficient amplitude along the entire grating length.

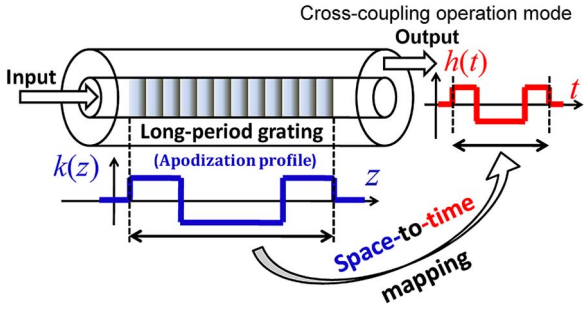

Fig. 3. Illustration of the space-to-time mapping phenomenon in LPGs. The illustrated design of $k(z)$ and the corresponding output temporal impulse response $h(t)$ in this figure show the implementation of the specific case of a 2nd-order all-optical differentiator (i.e., $N = 2$) based on a phase-shifted LPG.

Fig. 2(c) can be implemented based on LPGs with uniform (constant) coupling coefficient amplitude along the entire grating length. This significantly facilitates the fabrication of these LPG devices while increasing their tolerance against variations in the coupling strength along the grating length.

3.2. Grating Design Using the Space-to-Time Mapping Approach in LPGs

It has been recently demonstrated that, similar to the case of fiber/waveguide Bragg gratings (BGs) [21], [22], under certain conditions (first-order Born approximation), the cross-coupling time-domain impulse response $h(t)$ of an LPG is approximately proportional to the complex coupling coefficient profile along the grating length z (e.g., the grating apodization profile in Fig. 3, $k(z)$) after a suitable space-to-time scaling [15], [16]. The magnitude of $k(z)$ accounts for variations in the grating coupling strength along the device length (i.e., variations in the amplitude of refractive index modulation in a fiber LPG), whereas the phase of $k(z)$ accounts for discrete and continuous

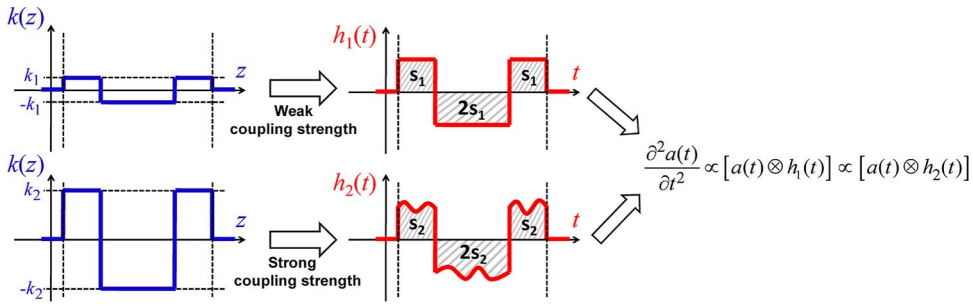

Fig. 4. Illustration of the effect of the coupling strength for implementation of NOODs (i.e., $N = 2$ in this example) based on the space-to-time mapping concept in LPGs. It is assumed that k_1 induces weak coupling whereas k_2 induces strong coupling.

variations in the local grating period profile. This space-to-mapping phenomenon is illustrated in Fig. 3, and it can be mathematically expressed as follows:

$$h(t) \propto k(z)|_{z=vt} \tag{4}$$

where the scaling factor v represents the space-to-time mapping speed. In LPGs, this mapping speed can be expressed as $v = c/\Delta N$, where $\Delta N = (n_{\text{eff1}} - n_{\text{eff2}})$, with n_{eff1} and n_{eff2} being the effective refractive indices of the two coupled modes around the wavelength of interest. Clearly, ΔN can be made much smaller than 1, and consequently, the resulting mapping speed can be made significantly higher than the speed of light in vacuum [15], [16]. This superluminal space-to-time mapping speed is thus considerably higher than the corresponding (subluminal) speed in the case of BG devices [21], [22], i.e., $v = c/(2n_{\text{eff}})$, where n_{eff} is the average effective refractive index of the propagating mode in the grating. This key feature enables the synthesis of temporal impulse responses with ultrafast temporal features (e.g., in the femtosecond range) using significantly relaxed spatial resolutions, easily above a few millimeters. This approach is used in our work to synthesize the temporal impulse responses defined in Fig. 2(c) for optical Nth-order differentiators with sampling periods in the femtosecond regime (corresponding to bandwidths exceeding a few THz) using centimeter-long LPGs.

In general, the condition of the first-order Born approximation in LPGs is referred to as weak-coupling strength condition [15], [16], which is strictly satisfied when the coupling coefficient peak is much lower than that at full-coupling condition, namely, $\max\{k(z)L\} \ll \pi/2$. This essentially means that the cross-coupling transfer function peak keeps smaller than $\sim$10%. However, as numerically demonstrated below, the first-order Born approximation does not need to be satisfied for implementation of the specific designs proposed here. As illustrated in Fig. 4, the resulting temporal impulse response for a high coupling coefficient is a distorted version of the ideal temporal impulse response (mapped version of the grating coupling profile). The distortion happens in a very similar fashion over each positive/negative section of the LPG's temporal impulse response in such a way that the ratios of the "areas" corresponding to each of these sections is kept nearly unchanged with respect to those of the ideal case. These ratios are actually the key factors in defining the proper convolution operation; as a result, the strong-coupling gratings can still provide very nearly the desired differentiation functionality. This described behavior has been observed in all our simulated designs, and it helps in ensuring that the designed differentiation devices offer the desired performance over an extended range of coupling coefficient values.

4. LPG Designs and Numerical Simulations

The optical waveguide platform for implementation of LPGs is considered to be the standard single-mode fiber (Corning SMF-28). The LPG design parameters are assumed to be the same as for the experimentally characterized LPG fabricated on SMF-28 in [23]. The grating period is $\Lambda = 430$ μm,

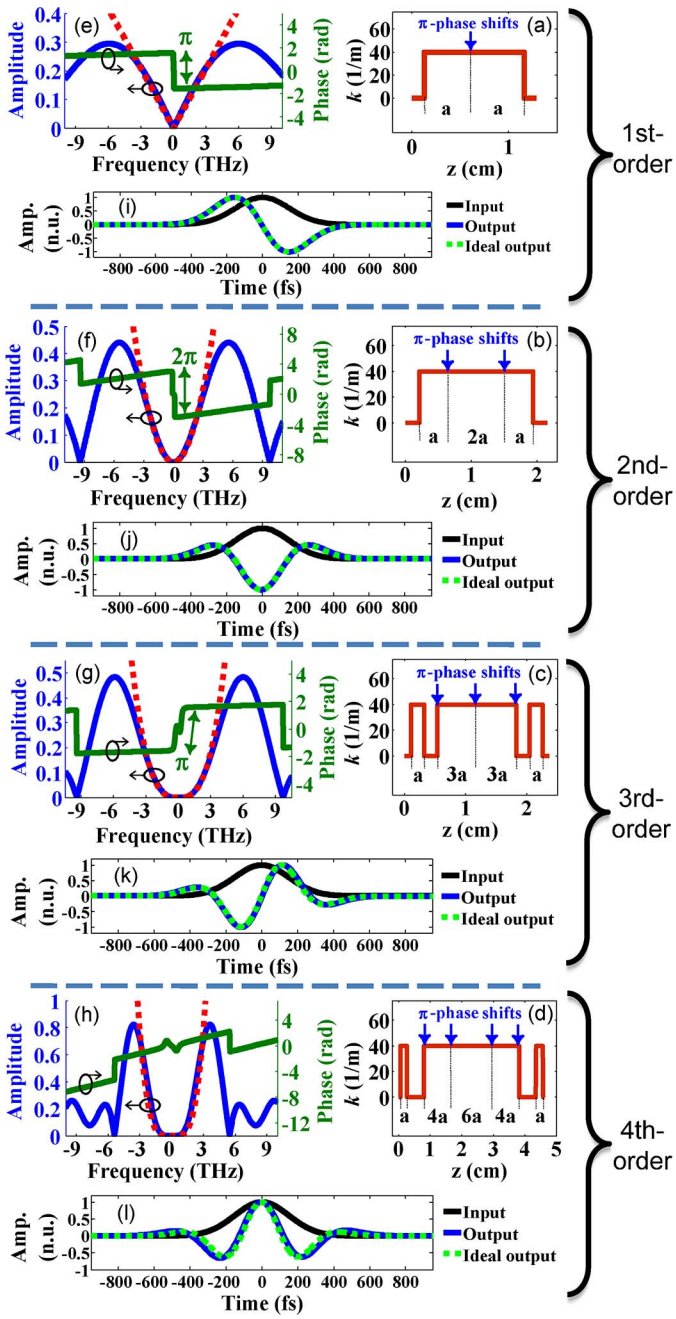

Fig. 5. (a)–(d) Phase-shifted LPG designs (local coupling coefficient) for implementation of 1st-, 2nd-, 3rd- and 4th-order ultrafast optical differentiators, respectively. (e)–(h) Corresponding simulation results for the spectral amplitude and phase responses of the designed phase-shifted LPGs shown with the solid curves. The ideal spectral amplitude response for each case is shown with the dotted curve. (i)–(l) Corresponding simulation results (solid, blue curves) for the temporal responses (complex envelopes) of the designed LPGs to an input ultrashort Gaussian pulse (250 fs-FWHM, shown with a solid, black curve), compared with the ideal numerical derivatives of the input pulse (dotted, green curves).

which corresponds to coupling of the fiber core mode into the LP06 cladding mode at a central wavelength of 1550 nm [23]. In the numerical simulations, the actual wavelength dependence has been considered for the effective refractive indices of the two coupled modes [23]: $n_{0,1}(\lambda) = 1.4884 - 0.031547\lambda + 0.012023\lambda^2$ for the core-mode and $n_{0,6}(\lambda) = 1.4806 - 0.025396\lambda + 0.009802\lambda^2$ for

TABLE 1

Estimated upper (BW_{max}) and lower (BW_{min}) limits of the acceptable ISB range for the designed LPG-based differentiators in Fig. 5(a)–(d). The input is considered to be a Gaussian pulse.

	1st-order	2nd-order	3rd-order	4th-order	5th-order	6th-order
BW_{min}	0.2THz	1.7THz	2.9THz	4.1THz	5.1THz	5.7THz
BW_{max}	9.2THz	9.4THz	7.5THz	7.7THz	6.4THz	6.5THz
BW_{max}- BW_{min}	9.0THz	7.7THz	4.6THz	3.6THz	1.3THz	0.8THz

the LP06 cladding-mode, where $1.2 < \lambda < 1.7$ is the wavelength variable in μm. The responses of LPGs are simulated using coupled-mode theory combined with a transfer matrix method [24].

Fig. 5(a)–(d) shows the LPG designs based on our proposed approach for implementation of 1st-, 2nd-, 3rd-, and 4th-order optical differentiators with a target operation bandwidth of $\sim$6 THz. These plots show the complex coupling coefficient versus length of the grating, i.e., amplitude of the grating apodization profile including the required π-phase shifts along the grating structure, for each of the LPG design. The cited values in Fig. 5(a)–(d), which are normalized as a multiple of a unit area called *a*, refer to the *areas* of the positive and negative parts of the temporal impulse response of the corresponding NOOD. The designed LPGs for implementation of the NOOD with $N = 1, 2, 3,$ and 4 have lengths of 1 cm, 1.7 cm, 2.1 cm, and 4.5 cm, respectively.

The numerically simulated spectral amplitude and phase responses of the designed LPGs are presented in Fig. 5(e)–(h), respectively. To confirm that the designed LPGs in Fig. 5(a)–(d) can operate as NOOD over the target device operation bandwidth (DOB), i.e., $\sim$6 THz, the time-domain responses to an ultrashort input Gaussian pulse is investigated. As discussed in [25], optical differentiators have a certain acceptable range for the input signal bandwidth (ISB). This acceptable ISB range is normally estimated based on the level of similarity, e.g., cross-correlation coefficient (C_c) defined in Section 5 below, between the actual differentiator's time-domain output and the corresponding ideal output [25]. In general, the acceptable ISB range covers a region from a certain bandwidth smaller than the DOB (i.e., defined as BW_{min}) to a certain bandwidth larger than DOB (i.e., defined as BW_{max}), i.e., $BW_{min} < ISB < BW_{max}$ (see [25] for more details). Table 1 presents the estimated minimum and maximum acceptable ISBs, i.e., BW_{min} and BW_{max}, respectively, for the designed LPG-based differentiators in Fig. 5(a)–(d), by considering a $C_c \geq 97\%$. Table 1 also includes the estimated BW_{min} and BW_{max} for two more cases of 5th- and 6th-order optical differentiators. It can be clearly seen that the acceptable ISB range, i.e., $BW_{max} - BW_{min}$ in Table 1, becomes narrower as the differentiator order is increased. More detailed analysis can be found in [25].

The input Gaussian pulse bandwidth (i.e., ISB) is assumed to be the full width at 0.2% of the amplitude spectrum peak. Concerning the time-domain outputs in Fig. 5, we have chosen ISB to be $\approx$6 THz. The corresponding temporal responses of the designed LPGs to the mentioned ultrashort (i.e., 250-fs intensity FWHM or ISB$\approx$6 THz) input Gaussian pulse are shown in Fig. 5(i)–(l), respectively. Our numerical simulations clearly confirm that the designed LPGs provide very nearly the required spectral responses and predicted temporal responses.

The tolerance of the proposed designs against variations in the grating coupling strength (i.e., *k*) is estimated by numerically simulating their respective spectral amplitude responses for different amounts of *k*. Fig. 6 shows the results of this simulation for the cases of 1st- and 2nd-order differentiators. As it can be seen in Fig. 6, even when the coupling strength is tuned over a very wide range of values, the designed LPGs maintain the required spectral response profiles along the DOB (linear amplitude variation for the 1st-order differentiator, and quadratic amplitude variation for the 2nd-order differentiator). Obviously, the cross-coupling peak amplitude response is increased for a higher value of *k*, additionally leading to an improved energetic efficiency of the device. Further performance evaluations of the proposed LPG-based differentiators are presented in Section 5.

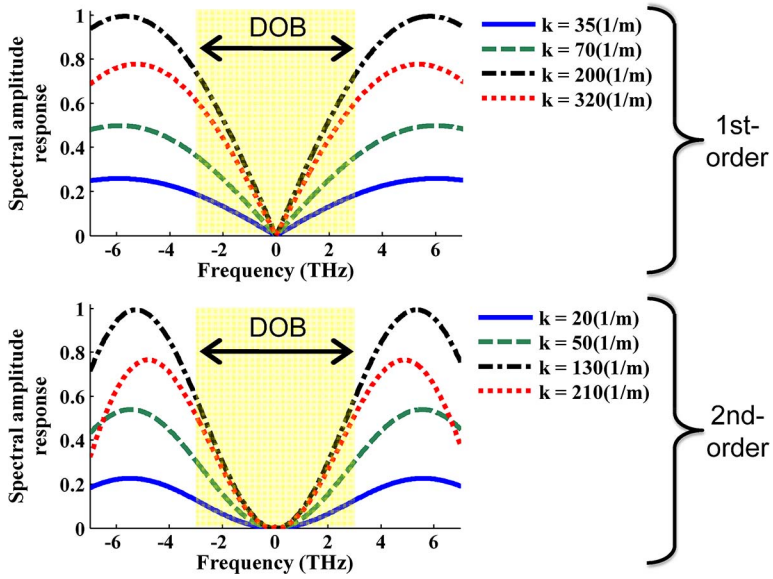

Fig. 6. Simulated spectral amplitude responses of the designed 1st- and 2nd-order differentiators based on the proposed phase-shifted LPGs working in the cross-coupling operation mode for different amounts of coupling strength (i.e., k).

5. Performance Evaluation of the Designed LPG-Based Differentiators

For our performance evaluations, the above defined ultrashort (i.e., 250-fs intensity FWHM corresponding to ISB $\simeq$ 6 THz) input Gaussian pulse is numerically launched at the input of the designed differentiator devices. Then, the device performance is fully evaluated by changing the LPG's coupling strength (i.e., k) and estimating: (i) the *level of similarity* between the actual LPG's time-domain output and the corresponding ideal output and (ii) the *energetic efficiency* performance. The mentioned *level of similarity* is estimated by using the cross-correlation coefficient (C_c) between the ideal output (i.e., Nth-order numerical derivative of the input time-domain waveform) and the actual LPG's output, defined as follows [26]:

$$C_c = \frac{\int_{-\infty}^{+\infty} P_{out}(t) P_{ideal}(t)\, dt}{\sqrt{\left(\int_{-\infty}^{+\infty} P_{out}^2(t)\, dt\right)\left(\int_{-\infty}^{+\infty} P_{ideal}^2(t)\, dt\right)}} \times 100\% \tag{5}$$

where $P_{\text{out}}(t)$ and $P_{\text{ideal}}(t)$ are the time-domain intensity profiles of the LPG's output and the ideal output, respectively. As mentioned above, the acceptable range of the coupling strength values is defined by considering a minimum value for the cross-correlation coefficient, e.g., $C_c \geq 97\%$. The *energetic efficiency* performance is estimated as the ratio between the energetic efficiency of the designed LPGs to the energetic efficiency of the ideal passive differentiator with 100% maximum amplitude spectral response and the same operation bandwidth. We refer to this parameter as energetic efficiency ratio (EER). Notice that the EER can indeed be larger than 100% since the power attenuation at the resonance dip of the ideal passive differentiator can be higher than that for the corresponding physically realizable (LPG-based) differentiator.

Fig. 7 summarizes the results of our performance evaluations for the newly proposed LPG-based ultrafast optical differentiator designs, as well as for the previously demonstrated (conventional) LPG approach in [11] and [13], for the cases of the NOODs with $N = 1, 2, 3,$ and 4. As anticipated, the newly proposed designs are nearly insensitive to variations in the LPG's coupling strength over extremely large coupling ranges; this compares very favorably with the significantly narrower tolerance to deviations in the coupling-strength value observed for previous LPG designs [11], [13].

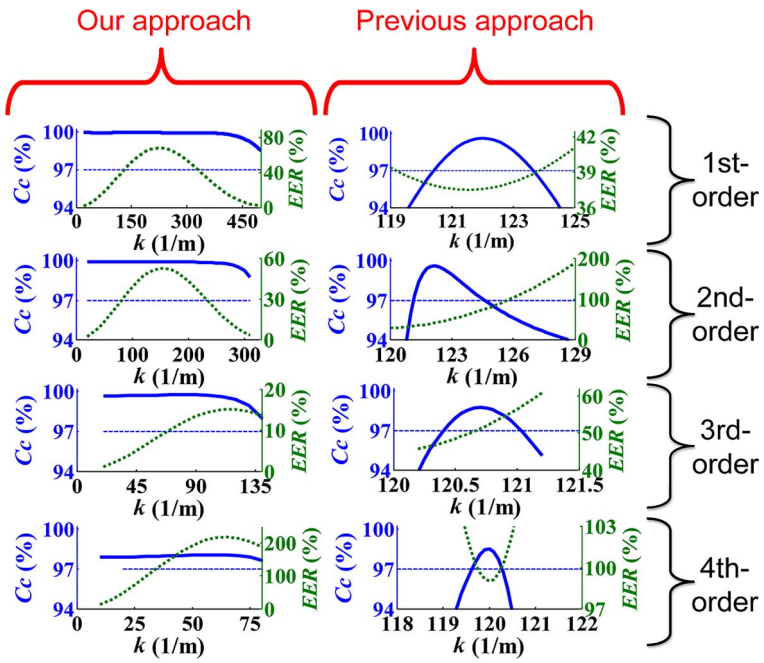

Fig. 7. Simulation results of C_c (solid blue curves) and *EER* (dotted green curves) as a function of the grating coupling strength (k) for the LPG-based ultrafast optical differentiator designs proposed here and using a previously demonstrated (conventional) approach [11], [13].

6. Tolerance of the Practical Fabrication Errors

In fiber grating fabrication techniques, the photo-induced LPGs can be inscribed into an optical fiber using either an amplitude mask or a point-by-point writing approach [27]–[29]. For the implementation of a NOOD in this paper, N π-phase shifts should be suitably inserted along the LPG's length. To induce a π-phase shift during the fabrication at a desired point, the translation stage is moved by 0.5 or 1.5 times the LPG period [28]. The precision for achieving a certain amount of phase shift in fiber grating fabrication depends on the positioning resolution of the translation stage [28]. In this regard, motorized translation stages provide more precise positioning as compared to stages controlled manually [30]. Typical nano-positioning linear translation stages provide positioning resolutions in nm range with a few mm travelling range [30]. Stages having tens of mm travelling range typically provide hundreds of nm positioning resolutions [30]. Here, we investigate the effect of the resolution of the translation stage in the fiber grating fabrication setup on the inserted π-phase shifts along the LPGs, which in turn affects the performance of the proposed optical differentiators.

Let us assume a positioning resolution of $\sim$1000 nm, which is notably worse than what is practically achievable in fiber grating fabrication setups [28], [30]. Therefore, the positioning error (PE) can be considered as $PE = \pm 1$ μm. The effect of PE on the implementation of a π-phase shift in the LPGs can be considered as a phase-shift deviation (PSD) from π, and it can be expressed as [28]

$$PSD = PE \times \pi/(\Lambda/2) \tag{6}$$

where Λ is the grating period, e.g., $\Lambda = 430$ μm has been assumed in this paper. For the positioning error of $PE = \pm 1$ μm the phase-shift deviation from π is estimated as $PSD \approx \pm 0.005\pi$. Thus, clearly, the positioning tolerance of the translation stages in practical fiber-grating fabrication setups is much shorter than the required half a grating period shift (e.g., 215 μm) for implementation of a π-phase shift in the LPGs [28]. Fig. 8 shows our simulation results for the

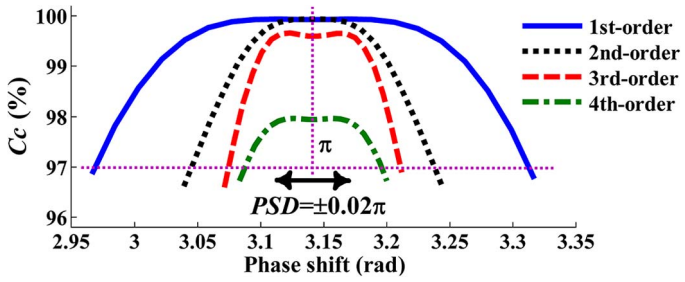

Fig. 8. Simulation results showing the effect of the phase-shift deviation (i.e., *PSD*) from π on the performance of the proposed π-phase-shifted LPG-based optical differentiators.

effect of the phase-shift deviation from π on the performance of the proposed π-phase-shifted LPG-based optical differentiators. For these performance evaluations, the same input pulse as that defined in Section 5 has been considered. It is worth noting that, for a desired minimum value of the cross-correlation coefficient, e.g., $C_c \geq 97\%$, higher-order differentiators have narrower tolerance ranges on the phase-shift deviation. Nonetheless, it can be seen from Fig. 8 that, even for phase-shift deviations significantly larger than $\pm 0.005\pi$, e.g., $PSD = \pm 0.02\pi$ as shown in the figure, the performance of the proposed NOODs $(N = 1, 2, 3, 4)$ suffer a nearly negligible degradation, smaller than 0.2% in all cases.

7. Conclusion

We have proposed and numerically demonstrated a novel design approach for THz-bandwidth arbitrary-order optical differentiators based on phase-shifted LPGs. The proposed designs offer a dramatically increased tolerance to deviations in the grating's coupling strength, thus overcoming the very narrow tolerance to deviations in the grating parameters suffered by previous designs. Our simulations have also shown that this design approach can provide processing bandwidths of up to several THz using readily feasible LPG specifications.

References

[1] M. H. Asghari, *Ultrafast Optical Signal Processing: Devices and Techniques*. Saarbrücken, Germany: LAMBERT Academic Publishing, 2012.
[2] J. Azaña, "Ultrafast analog all-optical signal processors based on fiber-grating devices," *IEEE Photon. J.*, vol. 2, no. 3, pp. 359–386, Jun. 2010.
[3] E. Palushani, H. Hu, L. K. Oxenlwe, R. Slavík, M. Galili, H. C. H. Mulvad, A. T. Clausen, and P. Jeppesen, "640 Gb/s timing tolerant demultiplexing using a cascaded long-period fiber grating pulse shaper," presented at the Eur. Conf. Optical Communication (ECOC), Vienna, Austria, 2009, Paper 4.3.3.
[4] A. Consoli, J. M. G. Tijero, and I. Esquivias, "Time resolved chirp measurements of gain switched semiconductor laser using a polarization based optical differentiator," *Opt. Exp.*, vol. 19, no. 11, pp. 10 805–10 812, May 2011.
[5] R. T. Watts, K. Shi, and L. P. Barry, "Time-resolved chirp measurement for 100GBaud test systems using an ideal frequency discriminator," *Opt. Commun.*, vol. 285, no. 8, pp. 2039–2043, Apr. 2012.
[6] F. Liu, T. Wang, L. Qiang, T. Ye, Z. Zhang, M. Qiu, and Y. Su, "Compact optical temporal differentiator based on silicon microring resonator," *Opt. Exp.*, vol. 16, no. 20, pp. 15 880–15 886, Sep. 2008.
[7] M. Li, D. Janner, J. Yao, and V. Pruneri, "Arbitrary-order all-fiber temporal differentiator based on a fiber Bragg grating: Design and experimental demonstration," *Opt. Exp.*, vol. 17, no. 22, pp. 19 798–19 807, Oct. 2009.
[8] L. M. Rivas, S. Boudreau, Y. Park, R. Slavıacute;k, S. Larochelle, A. Carballar, and J. Azaña, "Experimental demonstration of ultrafast all-fiber high-order photonic temporal differentiators," *Opt. Lett.*, vol. 34, no. 12, pp. 1792–1794, Jun. 2009.
[9] D. Gatti, T. T. Fernandez, S. Longhi, and P. Laporta, "Temporal differentiators based on highly-structured fibre Bragg gratings," *Electron. Lett.*, vol. 46, no. 13, pp. 943–945, Jun. 2010.
[10] K. A. Rutkowska, D. Duchesne, M. J. Strain, R. Morandotti, M. Sorel, and J. Azaña, "Ultrafast all-optical temporal differentiators based on CMOS-compatible integrated-waveguide Bragg gratings," *Opt. Exp.*, vol. 19, no. 20, pp. 19 514–19 522, Sep. 2011.
[11] R. Slavík, Y. Park, M. Kulishov, R. Morandotti, and J. Azaña, "Ultrafast all-optical differentiators," *Opt. Exp.*, vol. 14, no. 22, pp. 10 699–10 707, Oct. 2006.
[12] M. Li, H. S. Jeong, J. Azaña, and T. J. Ahn, "25-terahertz-bandwidth all-optical temporal differentiator," *Opt. Exp.*, vol. 20, no. 27, pp. 28 273–28 280, Dec. 2012.

[13] M. Kulishov, D. Krcmarík, and R. Slavík, "Design of terahertz-bandwidth arbitrary-order temporal differentiators based on long-period fiber gratings," *Opt. Lett.*, vol. 32, no. 20, pp. 2978–2980, Oct. 2007.
[14] J. Azaña and M. Kulishov, "All-fibre ultrafast optical differentiator based on π-phase-shifted long-period grating," *Electron. Lett.*, vol. 41, no. 25, pp. 1368–1369, Dec. 2005.
[15] R. Ashrafi, M. Li, and J. Azaña, "Femtosecond optical waveform generation based on space-to-time mapping in long period gratings," in *Proc. IEEE Photon. Conf.*, 2012, pp. 104–105.
[16] R. Ashrafi, M. Li, S. LaRochelle, and J. Azaña, "Superluminal space-to-time mapping in grating-assisted co-directional couplers," *Opt. Exp.*, vol. 21, no. 5, pp. 6249–6256, Mar. 2013.
[17] J. Jiang, C. L. Callender, J. P. Noad, and J. Ding, "Hybrid silica/polymer long period gratings for wavelength filtering and power distribution," *Appl. Opt.*, vol. 48, no. 26, pp. 4866–4873, Sep. 2009.
[18] R. Slavík, M. Kulishov, Y. Park, and J. Azaña, "Long-period-fiber-grating-based filter configuration enabling arbitrary linear filtering characteristics," *Opt. Lett.*, vol. 34, no. 7, pp. 1045–1047, Apr. 2009.
[19] R. Ashrafi, M. Li, N. Belhadj, M. Dastmalchi, S. LaRochelle, and J. Azaña, "Experimental demonstration of superluminal space-to-time mapping in long period gratings," *Opt. Lett.*, vol. 38, no. 8, Apr. 15, 2013.
[20] D. V. Griffiths and I. M. Smith, *Numerical Methods for Engineers*. Boca Raton, FL, USA: CRC Press, 2006.
[21] H. Kogelnik, "Filter response of nonuniform almost-periodic structures," *Bell Syst. Tech. J.*, vol. 55, no. 1, pp. 109–126, Jan. 1976.
[22] J. Azaña and L. R. Chen, "Synthesis of temporal optical waveforms by fiber Bragg gratings: A new approach based on space-to-frequency-to-time mapping," *J. Opt. Soc. Amer. B*, vol. 19, no. 11, pp. 2758–2769, Nov. 2002.
[23] M. Smietana, W. J. Bock, P. Mikulic, and J. Chen, "Increasing sensitivity of arc-induced long-period gratings—Pushing the fabrication technique toward its limits," *Meas. Sci. Technol.*, vol. 22, no. 1, p. 015201, Jan. 2011.
[24] T. Erdogan, "Fiber grating spectra," *J. Lightwave Technol.*, vol. 15, no. 8, pp. 1277–1294, Aug. 1997.
[25] R. Ashrafi and J. Azaña, "Figure of merit for photonic differentiators," *Opt. Exp.*, vol. 20, no. 3, pp. 2626–2639, Jan. 2012.
[26] A. Papoulis, *The Fourier Integral and Its Applications*. New York, NY, USA: McGraw-Hill, 1962.
[27] R. Kritzinger, D. Schmieder, and A. Booysen, "Azimuthally symmetric long-period fibre grating fabrication with a TEM_{01}-mode CO_2 laser," *Meas. Sci. Technol.*, vol. 20, no. 3, p. 034004, Mar. 2009.
[28] R. Slavík, Y. Park, M. Kulishov, and J. Azaña, "Terahertz-bandwidth high-order temporal differentiators based on phase-shifted long-period fiber gratings," *Opt. Lett.*, vol. 34, no. 20, pp. 3116–3118, Oct. 2009.
[29] B. J. O'Regan and D. N. Nikogosyan, "Femtosecond UV long-period fibre grating fabrication with amplitude mask technique," *Opt. Commun.*, vol. 284, no. 24, pp. 5650–5654, Dec. 2011.
[30] [Online]. Available: http://www.newport.com